lubricants

MDPI

Article

Noise Prediction Study of Traction Arc Tooth Cylindrical Gears for New Generation High-Speed Electric Multiple Units

Zhaoping Tang [1], Zhenyan Chen [1], Jianping Sun [2,*], Menghui Lu [3] and Hui Liu [1]

[1] School of Mechatronics and Vehicle Engineering, East China Jiaotong University, Nanchang 330013, China; tzp@ecjtu.edu.cn (Z.T.); 2022038085500057@ecjtu.edu.cn (Z.C.); 2022038085500069@ecjtu.edu.cn (H.L.)
[2] School of Transportation Engineering, East China Jiaotong University, Nanchang 330013, China
[3] School of Information Engineering, East China Jiaotong University, Nanchang 330013, China; 2021068085400013@ecjtu.edu.cn
* Correspondence: 1654@ecjtu.edu.cn

Abstract: As the speed of the new generation of high-speed electric multiple units (EMU) increases, the requirements for vibration and noise reduction in traction gear trains are becoming higher and higher. Although most researchers have focused on the vibration mechanics analysis of gears, the actual noise has the most direct impact on passenger experience and safety. To address this problem, a new type of curved cylindrical gear is proposed to analyze the dynamic characteristics of the gear pair and predict its radiated noise based on the acoustic-vibration coupling theory using the finite element-boundary element method. Parametric modeling of the gear pair using CREO and assembly motion analysis were performed. ANSYS was used to analyze the stress distribution, inherent frequency, and inherent vibration pattern of the gear pair, and harmonic response analysis was performed using the modal superposition method to solve the displacement frequency response curve and vibration characteristics. ACTRAN was used to construct the free-field model, create acoustic excitation based on the acoustic-vibration coupling equation, set the field points, and predict radiated noise. The research results show that the noise is mainly concentrated in the tooth meshing area, and the root mean square RMS range of its sound pressure level value is 91–100 dB. Its dynamic characteristics and noise values are in line with the traction requirements of high-speed EMU, providing a new idea for improving the noise prediction of traction gears for new generation high-speed EMU, which in turn strongly support the noise control of high-speed EMU stock and thus improve the passenger experience and driving environment.

Keywords: high-speed EMU; arc tooth cylindrical gear; dynamics analysis; acoustic-vibration coupling; noise prediction

Citation: Tang, Z.; Chen, Z.; Sun, J.; Lu, M.; Liu, H. Noise Prediction Study of Traction Arc Tooth Cylindrical Gears for New Generation High-Speed Electric Multiple Units. *Lubricants* **2023**, *11*, 357. https://doi.org/10.3390/lubricants11090357

Received: 11 July 2023
Revised: 13 August 2023
Accepted: 16 August 2023
Published: 23 August 2023

1. Introduction

China's CR450 Science and Technology Innovation Project aims to develop a new generation of high-speed rail products with higher speed and better performance to consolidate the country's leading position in high-speed rail technology worldwide [1]. The maximum operating speed of the CR450 rolling stock is 450 km/h, which places higher requirements on the train's comfort, smoothness, and safety. The traction gear transmission system serves as the primary power source for the propulsion system of the train and is considered a significant contributor to the overall noise generated. Therefore, it is important to study a gear system with better transmission performance for noise control and the safe operation of high-speed EMU.

At present, the mainstream rolling stock in the world generally adopts a helical gear drive system, and scholars at home and abroad have conducted extensive research on its dynamic performance and noise prediction. Chen et al. used a dynamic model of locomotive-track coupling, considered the dynamic action of gearing, analyzed the power transmission path under traction or braking conditions, verified the accuracy of the model,

and revealed the effects of gearing and track geometric irregularities on locomotive vibration and dynamic meshing forces [2]. Jiang et al. modeled the dynamic coupling effects of a heavy-duty electric locomotive to study the vibration characteristics of tooth root crack faults and analyzed them using time-frequency analysis and the angular simultaneous averaging method. The results showed that the longitudinal vibration acceleration and dynamic meshing force can reflect the fault characteristics, and the processed vibration signals can effectively reflect the dynamic characteristics of the crack expansion in the locomotive system [3]. Wang analyzed the coupled torsional vibration response of a gear train in a vehicle-track vibration environment and investigated the effects of time-varying stiffness, nonlinear damping, wheel deformation, and wheel-track interaction on the system. The results indicate that the traction torque and gear eccentricity during vehicle acceleration significantly affect vibration amplitude and frequency [4]. Zhao et al. developed a three-dimensional time-domain modeling method using an explicit finite element method to simulate the transient meshing contact and wear processes of a gear pair, considering the effects of actual geometry, time-varying torque, and structural vibration on the contact state. The results show that the profiles of structural vibration and wear have a strong influence on dynamic engagement contact [5]. Yang et al. qualitatively analyzed the evolution of the dynamic response, excitation frequency, periodic motion, quasi-periodic motion, and chaotic motion of a helical gear system with six degrees of freedom by developing a dynamical model with wear fault parameters using a numerical integration method. Their results showed that wear faults affected the system differently at different frequencies [6]. Wang proposed a gearing system model that considers time-varying meshing stiffness, nonlinear tooth gap, transmission error, time-varying external excitation, and orbital irregularity and performed a quasi-static analysis to observe its nonlinear behavior. The results indicated that quasi-static analysis is applicable to the analysis of the nonlinear behavior of time-varying stochastic systems [7]. Sun Gang established a rigid-flexible coupled system dynamics model for a type of high-speed EMU to study the dynamic performance of the system under various operating conditions and its dynamic interactions with the main components of the vehicle system [8]. Tang established a parametric gear modification model by theoretically analyzing, numerically simulating, and designing optimization algorithm methods, and analyzed the traction gear transmission system of a high-speed EMU to study its dynamic characteristics, vibration response, and acoustic response [9]. Zhang et al. analyzed the dynamic performance of gear transmission under the excitation of irregular track geometry based on the gear transmission-locomotive-track coupling dynamics model and found that the gearbox suspension parameters have a significant influence on the transmission performance, which provides a reference for the optimal design of the suspension parameters of locomotive gear transmission [10]. Zhu et al. studied the dynamic evaluation indices of high-speed train traction gearboxes at different measurement points, including acceleration, vibration intensity, and air noise, by establishing a dynamic model of a high-speed train gear train system and conducting spectrum analysis and experiments, which provided an important basis for system optimization design and fault diagnosis [11]. Liu et al. proposed a combined finite element/boundary element model based on the modal acoustic transfer vector (MATV) method to predict the radiated noise of a gearbox and analyzed the modal acoustic contribution and acoustic transfer vector to determine the maximum field point [12]. Ren et al. proposed a method based on the impedance model and noise transfer function for fast prediction of the radiated noise characteristics of gearboxes under different operating conditions. The effects of different excitation components and noise transfer functions on the noise were analyzed using the gear-box-foundation coupled impedance model and vibro-acoustic coupled boundary element model. Their results showed that high-speed bearings were the main source of radiated noise [13]. Tengjiao et al. used numerical simulation to calculate the vibration response of a dynamic finite element model consisting of a gear-rotor-bearing-case coupling, and then used the vibration displacement results of the gearbox surface nodes as acoustic boundary conditions to establish an acoustic boundary model of the gearbox. Vibration

and radiated noise analyses of the gear system were performed, and the calculated results agreed well with the experimentally tested data [14]. Han et al. developed a dynamic model of a gear rotor bearing system to determine the effect of meshing excitation on the gearbox vibration and noise, and an acoustic boundary element method was used to predict the gearbox noise distribution [15]. Gunasegaran used a higher-order spectral analysis technique to obtain acoustic data from vibration and airborne sound signals from a gearbox using a bispectral analysis [16]. Recently, experts have also utilized digital twin technology to achieve good results in emerging areas such as dynamics in various industrial contexts. They have employed adversarial graph networks in the field of bearing troubleshooting and introduced vibration-based wear prediction enhancements for spur gears. Feng K et al. [17,18] introduced adversarial graph networks (DT-DAGN) to address the problem of rolling bearing fault diagnosis in the digital twin domain. In addition, they can accurately predict the expected life by monitoring and evaluating the gear surface degradation, which in turn can be applied to real gearbox wear assessment.

Complex tooth surface gears can provide a higher transmission efficiency and greater load capacity to adapt to harsh environmental conditions at higher speeds and loads. Scholars at home and abroad have begun to conduct research on dynamic performance and noise prediction for complex gear systems such as spiral bevel gears, herringbone gears, and bevel gears. A spiral bevel gear with a high-order tooth surface was proposed by Mu et al., who found through simulation analysis that, compared to a conventional high-contact-ratio spiral bevel gear, this gear can effectively reduce the LTE, MI, and dynamic load factor, but also enhance its dynamic performance at all speeds [19]. Yuan et al. developed a wide-face, double-helical gear vice model with modified tooth surfaces by combining compensating tooth surface modification with multi-objective optimization modification, which can improve the load distribution and reduce the fluctuation of the vibration excitation force [20]. A multitooth loaded contact analysis model was developed by Li et al. to determine the meshing force and contact pressure distribution of a spiral bevel gear set using conjugate gradients and fast Fourier transforms, and the transmission performance was evaluated iteratively [21]. Chen proposed a dynamic model of a spiral bevel gear drive based on ERSFDs with a new mathematical model of ERSFDs and an oil film pressure calculation method, which has a better control performance of nonlinear characteristics in the speed range and can be extended to all rotating machines [22]. By optimizing the meshing characteristics of a herringbone gear pair, Li et al. found that the vibration noise of complex tooth surface gear systems could be reduced, the jumping phenomenon eliminated, and the system motion became more regular [23]. Zou et al. proposed an improved herringbone gear pair with a more uniform load distribution between the teeth and a better nonlinear dynamic performance [24]. Using Hertzian contact theory, Zhijun et al. studied the contact strength of a circular tooth-traced cylindrical gear set and found that it has a high contact strength, and its transmission design can be improved by reducing the tooth trace radius and tooth width ratio and increasing the contact ratio [25]. Syzrantseva et al. used finite element analysis to compare the stress-strain conditions of circular and straight teeth at different shaft misalignment angles. The results showed that circular gears have a smaller overall displacement (27% reduction) and higher bending strength and durability (18% increase), thus verifying their advantages for application in high-load transmissions [26]. Syzrantseva et al. calculated the failure probability of curved gears by considering the bending endurance and using non-parametric statistical methods. The results showed that the use of curved gears can significantly reduce the probability of gear failure owing to tooth bending under heavy load conditions compared to cylindrical helical gears [27].

Conventional gearing systems are widely used in high-speed EMU, while gearing systems with complex tooth surfaces are less frequently used. At present, high-speed EMU traction drives are used in the traditional helical gear transmission mode. Owing to the large additional axial force of the helical gear transmission system, after a long-term, high-load operation of the rolling stock, the gearbox bearings exhibit a more serious

pitting and blackening phenomenon because of the high oil temperature, accompanied by gearbox seal failure, gear lubrication deterioration, gear noise increase, and service life reduction. The new involute arc cylindrical gear not only has the characteristics of good meshing performance, large overlap coefficient, and tooth contact strength, but also has the incomparable advantages of helical gears because its axial forces can cancel each other out, there is no additional axial force, and the tooth surface is arc-shaped and has better lubrication performance. Furthermore, existing gear noise prediction methods primarily rely on kinetic analyses, which speculate about the relationship between noise and kinetic parameters, yet they lack comprehensive acoustic validation. Based on the acousto-vibration coupling theory, the Finite element-boundary element method was used to analyze arc tooth cylindrical gear dynamics under continuous traction conditions and to predict the magnitude and location of the noise. The results prove that the gear design helps reduce vibration and noise, improves transmission efficiency and accuracy, and can be an ideal choice for a new generation of high-speed EMU.

2. Parametric Design of the Traction Arc Tooth Cylindrical Gear

2.1. Establish the Relevant Design Parameters of the Gear

Based on the operating conditions of the new generation of high-speed EMU and the helical gear design parameters of the CRH380A high-speed EMU, geometric parameters, such as the modulus, number of teeth, pressure angle, gear width, and tooth-top height coefficient of the curved cylindrical gears, were initially set (Table 1).

Table 1. Basic geometric parameters of gear pairs.

Name	Pinion	Large Gear
Number of teeth Z	37	82
Modulus mn/(mm)	5	5
Pressure angle α/(°)	20	20
Tooth width B/(mm)	70	70
Tooth top height factor HAX	1	1
Top gap coefficient CX	0.2	0.2
Outer edge angle R_2/(mm)	180	180
Inner edge angle R_1/(mm)	160	160

We defined the basic relational equation of the gear according to the parameters, constrained the basic circle using the relational equation, and defined the involute parametric equation (Equation (1)) in the default Cartesian coordinates of the CREO and mirrored it.

$$\begin{cases} x = r_b * \cos(theta) + r_b * \sin(theta) * theta * (\pi/180) \\ y = r_b * \sin(theta) - r_b * \cos(theta) * theta * (\pi/180) \\ z = 0 \end{cases} \quad (1)$$

where r_b is the radius of the base circle, and $theta$ is the involute spread angle.

2.2. Create Inner and Outer Edge Curved Tooth Line

Taking the plane of the arc-tooth line as the sketching plane, take the straight line where the intersection of the involute and the index circle is located as the reference, place the center of the circle on this straight line, draw a circle of radius R_1 so that it intersects with the intersection of the index circle and the involute and extends along the projection of the index circle; then, half of an internal arc-tooth line is obtained by trimming the width B. The same method was used to draw half of the outer arc, as shown in Figure 1.

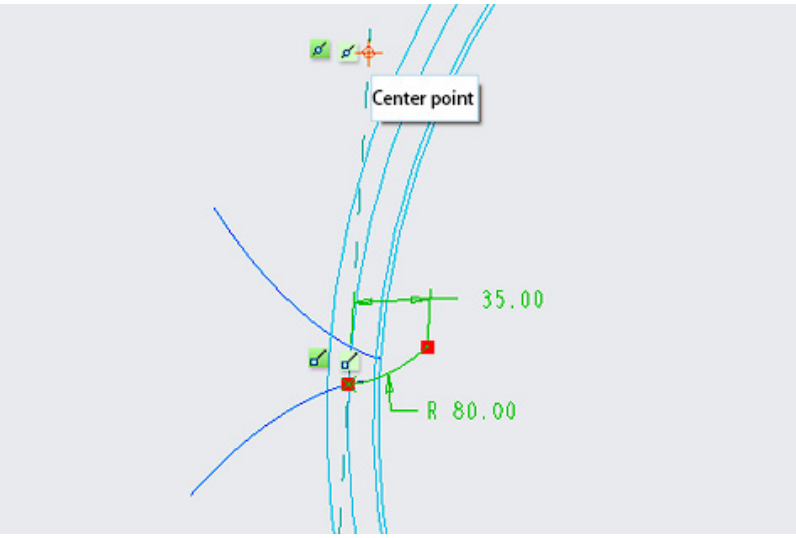

Figure 1. Inside and outside edge curved toothed line creation diagram.

2.3. Create Gear Blanks, Remove Half Teeth, Mirror, Combine an Array

Create the gear blank, remove half teeth, mirror, combine, and array, as shown in Figure 2.

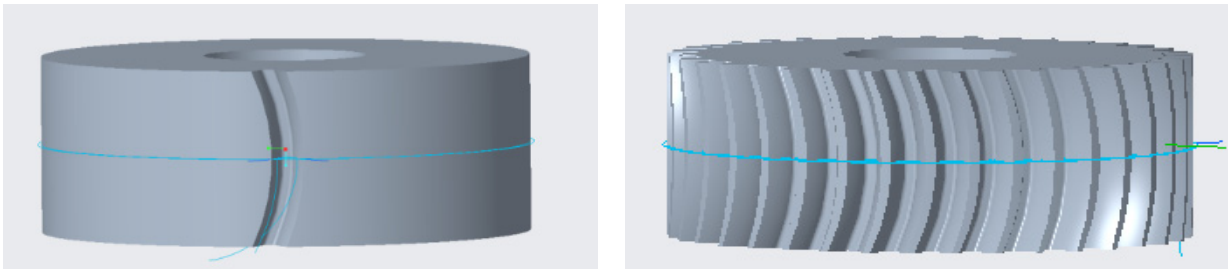

(**a**) (**b**)

Figure 2. (**a**) Half groove diagram; (**b**) post-groove array diagram.

Stretch to create the gear blank, and according to the shape of the tooth groove, use the involute, root circle, and top circle as the cross-section, and the inner and outer edge arc tooth line as the trajectory line. A constant cross-section and sweep perpendicular to the trajectory were selected to cut half of the tooth groove in the control panel, creating mirroring half-slots. The mirrored half slot was combined with the original half slot, and an axis array was created for the combination.

2.4. Perfecting the Gears

We created shaft planes, shaft holes, keyways, spokes, and other structures to perfect gears. The diameter of the journal at the gear mounting and the size of the key are determined based on the standard, and to satisfy the strength. Considering the workload of the simulation calculation, we ignored the drive shaft and other components, completed the pinion model, and generated another large gear based on the parameterized design of the pinion model.

2.5. Assembly and Motion Simulation Analysis

The CREO assembly mode adjusts the interference of the gear contact part, provides a pinion with a servo motor, and sets its speed to 434 °/s. Figures 3 and 4 show the speed and position of the top circle of the large and small gear teeth on the *Z*-axis.

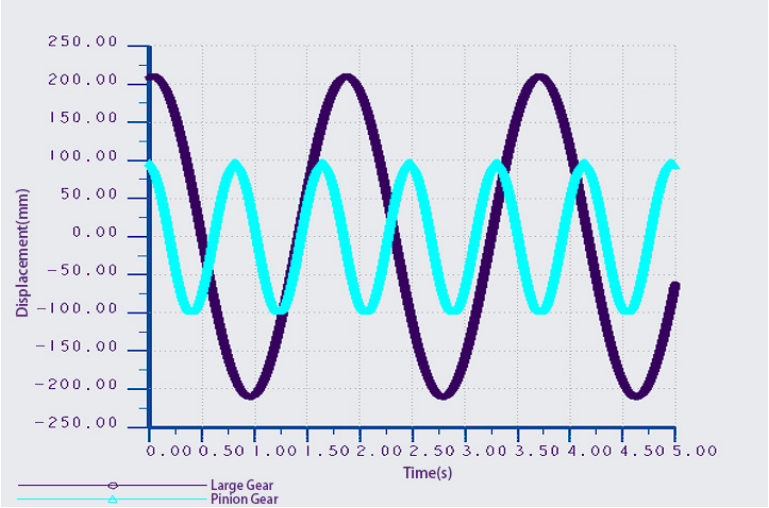

Figure 3. Graph and data of the position of the point on the top circle of the tooth of the large and small gears on the *Z*-axis.

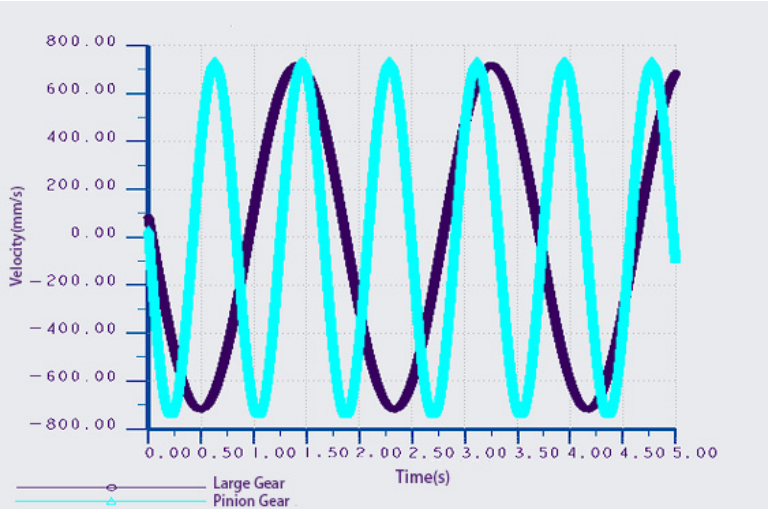

Figure 4. Graph and data of the velocity of a point on the top circle of a large and small gear tooth on the *Z*-axis.

The following is an analysis of the data from the size gear graphs. The position of the large gear measurement point is in the z-component range (−210–210 mm), the position of the pinion measurement point is in the z-component range (−97–97 mm), and the amplitude ratio of the large gear to the pinion coincides with the transmission ratio. The speed of both large and small gears in the z-component range is (−784–784 mm/s), which is the law of sine and cosine variation, and the ratio of the number of sine waves of small and large gears simultaneously coincides with the transmission ratio. Based on the simulation results, it can be concluded that the gear assembly is reasonable.

3. Gear Sub-Dynamic Analysis

A transient dynamic analysis of the arc tooth cylindrical gear model can be used to understand the state of stress and deformation during driving to further verify the adaptability of the gear under traction conditions. In this study, the ANSYS WORKBENCH transient module was selected to analyze the dynamics.

3.1. Define Geometric Models and Physical Properties

The gear pair model was imported, and the corresponding physical properties, such as modulus of elasticity, Poisson's ratio, and mass density, were set. Based on the material properties of the helical gear pair of the CRH380A high-speed EMU, the initial settings of the material properties of the arc tooth cylindrical gear pair are presented in Table 2.

Table 2. Gear material properties.

Material Properties	Pinion	Large Gear
Modulus of elasticity $E/(\mathrm{Pa})$	2.06×10^{11}	2×10^{11}
Poisson's ratio μ	0.31	0.3
Density $\rho/(\mathrm{kg/m^3})$	7850	7800

3.2. Grid Division

Mesh partitioning can make complex physical problems easier to solve numerically while reducing computational effort and improving computational efficiency. The higher the accuracy, the more accurate the results; however, the longer the calculation time is. In this paper, we choose a tetrahedral mesh that was more suitable for the gear shape and refined only the contact surfaces to save computational time while ensuring the accuracy of the results, and finally determine the number of nodes as 472,683.

3.3. Set up Solvers, Constraints, and Loads and Perform Simulation Calculations

Before performing the simulation, it was necessary to consider gear motion, forces, constraints, and loads to ensure the accuracy and reliability of the simulation results. To set the constraints, speed, and load of the gear pair as close as possible to those of the real state, we used a transient analysis. The constraint condition allows only the large gear and pinion to rotate, and the load condition sets the speed to be applied to the pinion and the torque to be applied to the large gear. Considering that the rolling stock usually operates under continuous operating conditions, this study sets the gear speed and torque of the new-generation high-speed EMU under continuous operating conditions, as shown in Table 3, and the load constraint, as shown in Figure 5.

Table 3. Gear vice working parameters.

Work Conditions	Torque (N/m)	Rotational Speed (Rad/s)
Continuous working conditions	814.5	434

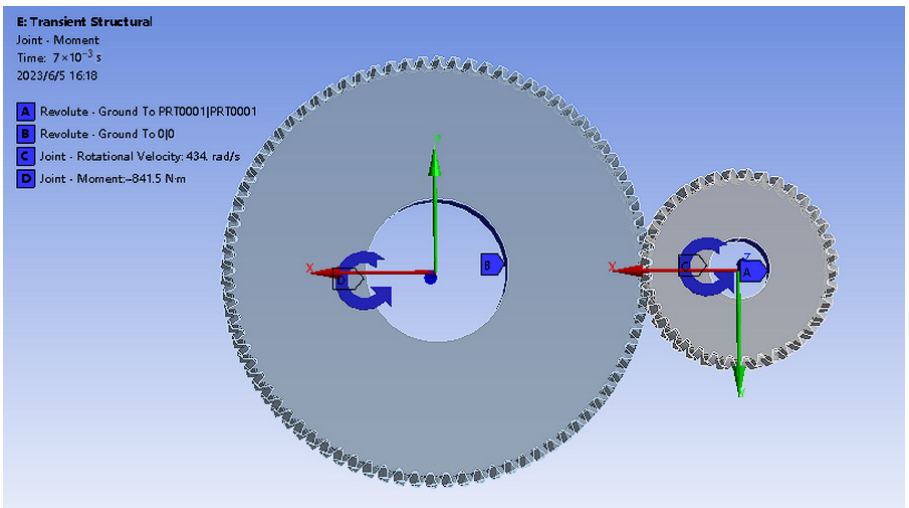

Figure 5. Gear vice load constraint.

3.4. Gearing Error Analysis

Gear transmission error is the error caused by gear axis displacement and tooth shape deviation due to manufacturing and assembly errors, as well as external excitation when gears mesh. These errors can lead to imperfect gear meshing, causing an uneven load distribution on the tooth surface, accelerating gear wear and damage, and generating gear vibrations and noise. Gear transmission errors can be divided into two types: dynamic and static errors, which are mainly caused by differences between the gear design and actual manufacturing, such as tooth shape deviation. Transmission error is one of the sources of whistling noise excitation; therefore, it must be analyzed.

The calculation of gear transmission error (TE) is typically based on the difference between two adjacent peaks in the output curve and the difference between the actual and theoretical rotational angles of the driven wheel in the same cycle during the actual meshing of the gear. This error significantly affected the vibration of the gear train. The theoretical expression is given by Equation (2):

$$TE = \frac{\theta_2 z_2}{z_1} - \theta_1 \tag{2}$$

where θ_1 denotes the pinion drive angle; θ_2 denotes the large gear drive angle; z_1 denotes the number of pinion teeth; and z_2 denotes the number of large gear teeth.

According to Equation (2) in the ANSYS workbench 2022 R1 software, the transmission error analysis of the traction arc tooth cylindrical gear pair under continuous working conditions is developed, and the linear error diagram of gear transmission is drawn as shown in Figure 6, and the specific data table is shown in Table 4.

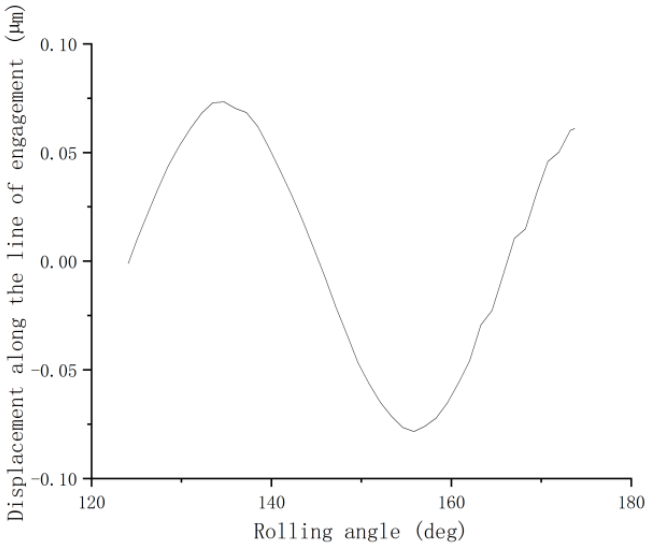

Figure 6. Gearing linearity error diagram.

Table 4. Gearing linear error data.

Extreme Values	Rolling Angle (°)	Displacement along the Line of Engagement (μm)
Maximum value	135	0.0732
Minimum value	156	−0.0784
Scope	21	0.1516

The linear plot of the gear drive error, as shown in Figure 6, represents the mesh curve of the gear in one meshing cycle in ANSYS software. The analysis in Table 4 shows that the gear transmission error value is 0.1516 μm, which is a very small transmission error and indicates that the traction arc tooth cylindrical gear exhibits an excellent meshing performance during transmission.

3.5. Stress Analysis

A stress analysis of the gears was performed to understand the forces acting on the gears under operating conditions and to assess their load-carrying capacity and deflections to optimize their design and ensure their reliability.

3.5.1. Contact Stress Analysis

Tooth contact can usually be considered as contact between two cylinders. In gear meshing, the tooth surfaces are in contact with each other and there is a stress distribution at the contact points. Therefore, the Hertzian formula was chosen to analyze the tooth contact stresses.

$$\sigma_{H_{\max}} = \sqrt{\frac{F_{ca}}{\pi b}\left(\frac{\frac{1}{\rho_1}+\frac{1}{\rho_2}}{\frac{1-\mu_1^2}{E_1}+\frac{1-\mu_1^2}{E_2}}\right)} \tag{3}$$

where ρ_1 and ρ_2 are the radii of curvature, F_{ca} is the total load acting on the contact line, b is the length of the meshing line, μ_1 and μ_2 are the Poisson's ratios of the large and small gear materials, respectively, and E_1 and E_2 are the moduli of elasticity of the large and small gear materials, respectively. According to Equation (3), the stress analysis of the gear pair was performed based on the contact tool of the ANSYS software. As shown in Figure 7, the tooth contact stress clouds at the entry, middle, and exit points of the gear are listed in Table 5.

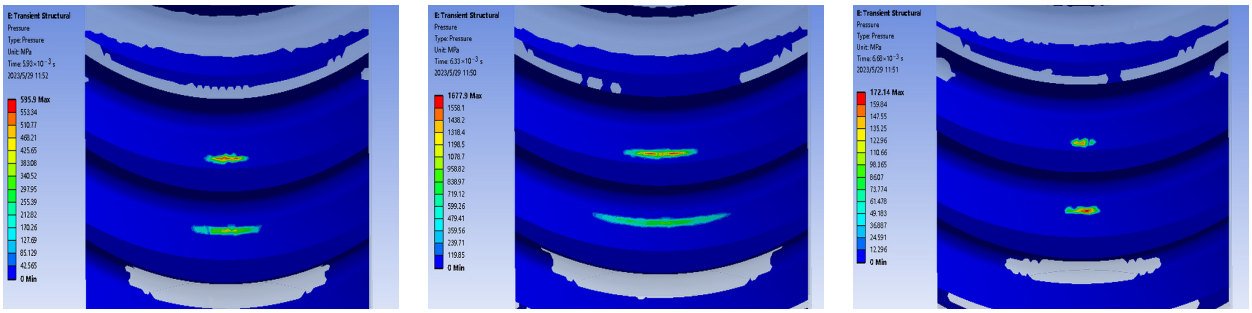

(**a**) (**b**) (**c**)

Figure 7. (**a**) Tooth surface contact stress cloud at the beginning of the engagement phase; (**b**) tooth surface contact stress cloud at the middle of the engagement phase; (**c**) tooth surface contact stress cloud at the separation phase of engagement.

Table 5. Maximum stress at each engagement.

Engagement Status	Contact Stress on the Tooth Surface (MPa)
Start of engagement phase	595.9
Mid-engagement phase	1677.9
Engagement separation phase	172.14

An analysis of Figure 7 illustrates how the tooth contact stresses change during the transient meshing of the large gear. The contact stress gradually increased and reached a maximum value of 1677.9 MPa from engagement to engagement and gradually decreased from engagement to the engagement process. The gear contact stress is distributed in the middle of the tooth surface, the contact length is longer, the contact area is larger, and the load distribution is more uniform. Compared to conventional gears, the curved tooth surface design of curved cylindrical gears helps reduce the stress concentration on the tooth surface and improves the load-carrying capacity of the gear.

3.5.2. Shear Stress Analysis along the Tooth Width Direction

During gearing, the tooth shape and torque cause relative sliding and shear forces between tooth surfaces, resulting in the generation of shear stress along the tooth width. The magnitude of the shear stress is related to the geometry of the gear, nature of the material, torque transmitted by the gear, and number of gear teeth, as shown in Equation (4).

$$\tau_w = K_s K_w K_f \frac{F_t}{b_w} \tag{4}$$

where τ_w represents the shear stress along the tooth width in units of N/mm^2; K_s is the tooth profile coefficient; K_w is the load factor; K_f is the stress correction factor; F_t is the torque transmitted by the gear in units of N, and b_w is the tooth width of the gear in mm.

Practical work, which is affected by various factors such as motor performance and manufacturing errors, will lead to a shear stress greater than the theoretical value, and there will be an uneven distribution of the actual maximum shear stress:

$$\tau_{w\max} = Y_R Y_{st} \tau_w = Y_R Y_{st} K_s K_w K_f \frac{F_t}{b_w} \tag{5}$$

where $\tau_{w\max}$ indicates the actual maximum shear stress along the tooth width, in N/mm^2; Y_R is the tooth-wise load distribution factor, and Y_{st} is the tooth width load distribution factor.

Equation (5) develops a shear stress analysis of a gear pair based on the ANSYS software, and the shear stress clouds during the meshing of the large gear and pinion are obtained, as shown in Figures 8 and 9. The specific data are presented in Table 6.

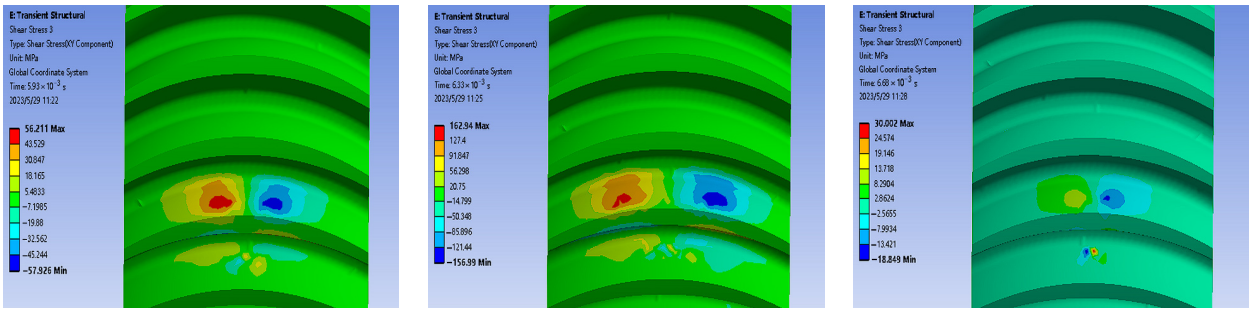

(**a**) (**b**) (**c**)

Figure 8. (**a**) Shear stress along the tooth width at the beginning of the pinion meshing phase; (**b**) shear stress along the tooth width in the middle phase of pinion meshing; (**c**) shear stress along the tooth width during the pinion meshing separation phase.

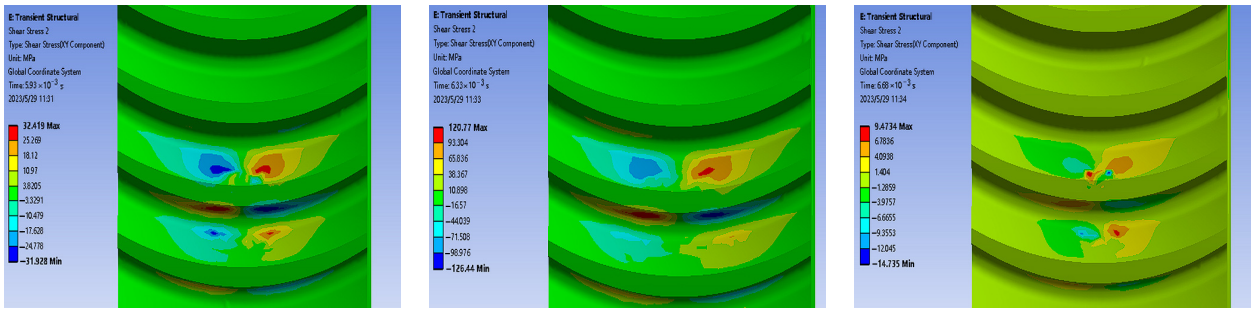

(**a**) (**b**) (**c**)

Figure 9. (**a**) Shear stress along the tooth width at the beginning of the large gear meshing phase; (**b**) shear stress along the tooth width at the intermediate phase of large gear meshing; (**c**) shear stress along the tooth width at the separation phase of the large gear meshing.

Table 6. Shear stress data table along the tooth width for large and small gears.

Engagement Status	Shear Stress of the Pinion along the Tooth Width Direction (MPa)	Shear Stress of Large Gears along the Tooth Width Direction (MPa)
Start of engagement phase	(−57.926, 56.211)	(−31.928, 32.419)
Mid-engagement phase	(−156.99, 162.94)	(−126.44, 120.77)
Engagement separation phase	(−18.849, 30.002)	(−14.735, 9.4734)

The analysis of Figures 8 and 9 shows the variation in the shear stresses during the meshing of the large and small gears in one transient meshing cycle. The stress gradually increased from engagement to mid-engagement, reached a maximum value, and then gradually decreased during the engagement-to-engagement-out process. Owing to the curved design of the tooth surface, the shear stress in the gear mesh is exhibited in opposite directions on both sides of the tooth surface. The tooth face on one side is subjected to positive shear stress, whereas that on the other side is subjected to shear stress in the opposite direction. This symmetrical distribution of shear stresses allows the axial component forces to cancel each other out, thereby reducing the load on bearings and shafts. The analysis in Table 6 shows that the actual shear stresses during pinion engagement, meshing, and meshing are −1.715 MPa, 5.95 MPa, and 11.153 MPa, respectively. The actual shear stresses during engagement, engagement, and disengagement of the large gear were 0.491 MPa, −5.67 MPa, and −5.2616 MPa, respectively. The combined analysis results show that, for pinions and large gears, the direction and magnitude of the shear stresses change at different stages during the meshing process. However, the overall view of the load distribution is more uniform in gear meshing, and it is not easy to produce meshing in and out of shock and vibration noise.

4. Modal Analysis

The gear pair is a key component of the gearbox and its vibration characteristics significantly affect the operation and noise of the entire system. By performing modal analysis on the gear pair, determining its vibration characteristics, such as inherent mode and inherent vibration pattern, comparing the inherent frequency and inherent mode, and optimizing the gear design, the resonance phenomenon can be effectively avoided, noise and vibration levels can be reduced, and a theoretical basis for subsequent gear noise prediction can be provided.

4.1. Modal Analysis Theory

In the finite element analysis program, the vibration equation is expressed as:

$$[M]\{x''\} + [C]\{x'\} + [K]\{x\} = \{f\} \tag{6}$$

where $[M]$ denotes the mass matrix, $[C]$ the damping matrix, and $[K]$ the stiffness matrix.

Setting the zero initial condition and performing the Laplace transform on the above equation yields.

$$\left(s^2[M] + s[C] + [K]\right)\{x(s)\} = \{F(s)\} \tag{7}$$

Treating in the Fourier domain, replacing s by ω, yields:

$$\left([K] - \omega^2[M] + j\omega[C]\right)X(\omega) = F(\omega) \tag{8}$$

For a linear system, the response is:

$$X_i(\omega) = \varphi_{i1} q_1(\omega) + \varphi_{i2} q_2(\omega) + \cdots + \varphi_{ir} q_r(\omega) \tag{9}$$

where $q_r(\omega)$ is the order modal coordinate, and φ_{ir} is the order modal vibration parameter of the measurement point.

The effect of the system damping on the modal state of the system itself is small; therefore, the effect of damping on the modal state of the system is neglected.

$$Mx'' + Kx = 0 \tag{10}$$

Assume that the solution is:

$$\{x\} = \{\varphi\} e^{iwt} \tag{11}$$

Substituting into Equation (10) yields the characteristic equation:

$$\left(K - \omega_n^2 M\right)\{\varphi\} = 0 \tag{12}$$

Equation (12) is the frequency equation for modal analysis and ω_n^2 is the eigenvalue. Arrange ω_n^2 in ascending order $0 \le \omega_1^2 \le \cdots \omega_i^2 \le \omega_n^2$, where ω_i denotes the i-th order intrinsic frequency of the structure itself. The $\{x\}_i$ denotes the vibration pattern corresponding to the ith-order intrinsic frequency.

4.2. Gear Sub-Modal Simulation

ANSYS WORKBENCH was used to implement the modal analysis of the system.

1. Create geometric model: import the gear subassembly model built in CREO.
2. Define material properties: in ANSYS, physical properties such as elastic modulus, Poisson's ratio, and mass density are defined.
3. Meshing: the accuracy of meshing has a great impact on the accuracy of simulation results. The method is consistent with that in transient analysis.
4. For modal analysis of gears, it is crucial to define the correct boundary conditions. To simulate the vibration characteristics of the gear pair in the actual operation more accurately, boundary conditions were defined to match the normal installation conditions of the gear pair as much as possible.
5. We define the modal analysis settings: in the gear system, the first 6th-order mode usually contains the most dominant vibration mode in the system; therefore, this study selects the first 6th order mode of the gear vice, solves the inherent frequency according to Equation (12), as shown in Table 7, and solves the inherent vibration pattern according to Equation (11), as shown in Figure 10.

Table 7. First 6th-order inherent frequency of the gear pair.

Order	Frequency (Hz)
1	7.3799
2	936.05
3	2315.8
4	2352.8
5	2545.4
6	2596.6

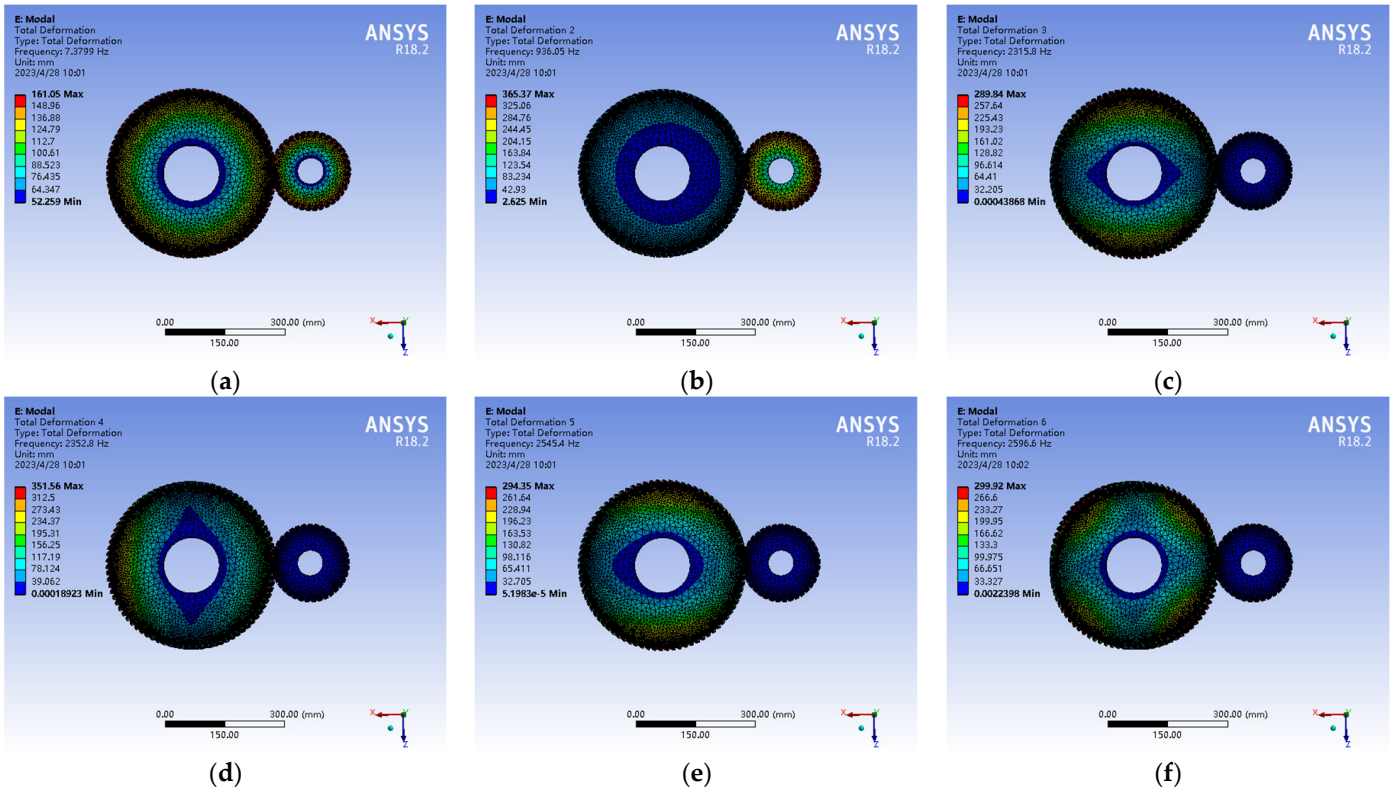

Figure 10. (**a**) First-order intrinsic vibration pattern; (**b**) second-order intrinsic vibration pattern; (**c**) third-order intrinsic vibration pattern; (**d**) fourth-order intrinsic vibration pattern; (**e**) fifth-order intrinsic vibration pattern; (**f**) sixth-order intrinsic vibration pattern.

5. Harmonic Response Analysis

Harmonic response analysis is an important pre-processing step before conducting gear-acoustic simulations. It is used to determine the displacement frequency response curve during operation and predict the vibration response characteristics of gears to improve their performance and reliability. It provides accurate input parameters for subsequent acoustic simulations, helping designers better understand the operating characteristics of gears and optimize their designs.

The harmonic response of an undamped system is often expressed using the forced vibration equation, as follows:

$$Mx'' + Kx = F \tag{13}$$

The harmonic response can be expressed as follows:

$$F = F_{i\max} \sin(\omega t + \phi) \tag{14}$$

where $F_{i\max}$ is the load amplitude, ω is the load angular frequency, and ϕ is the load phase angle.

Where x is:

$$x = x_h + x_p \tag{15}$$

where x_h is a general solution of the chi-square equation and x_p is a special solution of the non-chi-square equation.

Substituting (14) and (15) into (13) yields the inherent frequency of the load.

$$f = \frac{1}{2\pi}\sqrt{\frac{k}{m_{eff}}} \tag{16}$$

where k is the stiffness of the system and m_{eff} is the equivalent mass of the object under force.

Resonance analysis is typically performed by comparing the ratio of the actual damping ratio of the system to the critical damping ratio.

The actual damping ratio is calculated as:

$$\xi = 2c\sqrt{\frac{\rho E}{G}} \tag{17}$$

where c denotes the damping ratio, ρ denotes the material density, E denotes the elastic modulus of the material, and G denotes the shear modulus of the material.

The critical damping ratio is calculated as:

$$\xi_c = \frac{f}{2\sqrt{\frac{k}{m}}} \tag{18}$$

By correlating the above theories, ANSYS WORKBENCH harmonic response analysis was used, and the specific steps are as follows:

1. Based on the modal analysis, the harmonic response analysis is performed based on the modal superposition method, as shown in Figure 11.
2. Applied load: in the actual working condition, the gear pair is usually subject to the action of the rotating moment; therefore, according to Equation (14), the moment load is applied to the large gear to improve the accuracy and reliability of the analysis results and simulate the vibration response characteristics of the gear pair under actual working conditions.
3. Solve and observe the results: solve the vibration response characteristics of the transmission gear according to Equations (15) and (16), and observe the output displacement frequency response curve, as shown in Figure 12.

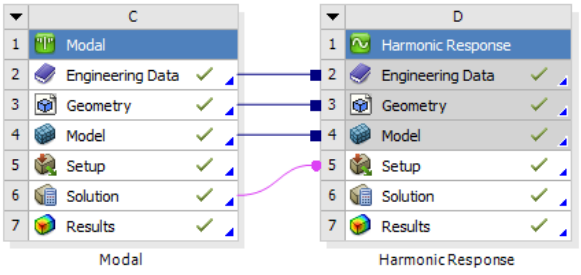

Figure 11. Modal superposition method.

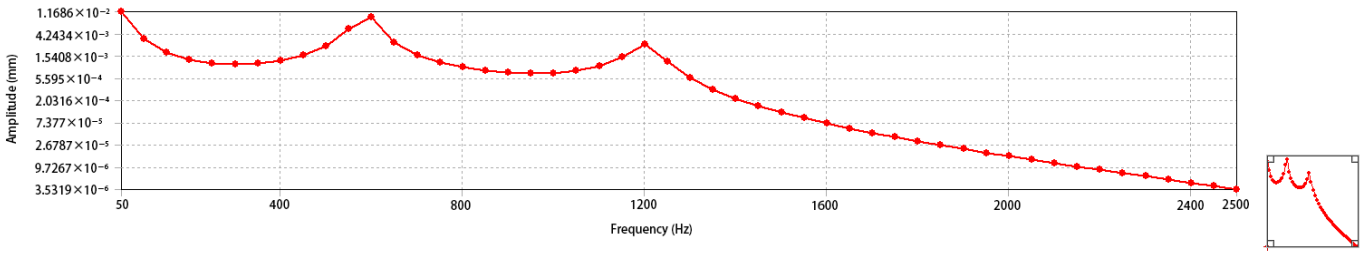

Figure 12. Displacement frequency response curve.

At 600 and 1200 Hz, the frequency response curve has a large peak, which is in line with the situation where the vibration in the gearing process presents a multiplication of frequencies. Combined with Table 4, it is found that 600 Hz and 1200 Hz avoid the inherent frequency of the system because the inherent frequency of the gear pair is under the ideal condition of no damping and no load, whereas the harmonic response analysis considers the actual external load, boundary conditions, and structural damping, which

can cause the actual response to differ from the modal analysis results. According to Equations (17) and (18), the damping ratio is greater than the critical damping ratio, which means that the gear pair is well damped and the vibration will gradually decay without resonance.

6. Noise Analysis

A curved cylindrical gear pair was analyzed using the ACTRAN workbench 2022 R1 software. Based on the vibration response characteristics, a boundary element method of solutions based on acoustic theory analysis is used to calculate the acoustic data of the gear subsurface and field points. A complete simulation process, from dynamics to acoustics, was developed to provide a more reliable noise prediction method for next-generation trains.

6.1. Selection of Acoustic Numerical Calculation Methods

The acoustic aspects of structural vibrations are the interrelationships between structural vibrations and sound. Structural vibration generates sound, and sound causes structural vibration, which are two different problems in engineering but are one in mechanical expression, differing only in the inputs to the mechanical system. Through motion and pressure, the structural and sound field control equations were coupled in a finite element model.

The finite element dynamics equations for structural vibration are shown in Equation (13).

By defining a model for the propagation of sound waves, they are typically represented by the Helmholtz equation.

$$\nabla^2 p + k^2 p = 0 \tag{19}$$

where ∇ denotes the Laplace operator, p denotes sound pressure, and k denotes wavenumber.

Sound waves propagate through the surface of a structure, and the sound pressure on the surface is expressed as:

$$p(x,t) = p_0(x)e^{j\omega t} \tag{20}$$

where $p_0(x)$ denotes the sound pressure on the surface of the structure, ω denotes the angular frequency, and j denotes the imaginary unit.

Acoustic-structural coupling boundary conditions were defined. The displacement on the surface of the structure was coupled with the sound pressure as follows:

$$p_0(x) = -Z(x)\left\{\frac{d(x,t)}{dx}\right\} \tag{21}$$

where $Z(x)$ is the acoustic impedance of the structure and $\frac{d(x,t)}{dx}$ is the displacement gradient of the structure surface.

Concerning the coupling of structural vibration and acoustic wave propagation models, substituting Equations (20) and (21) into Equations (13) and (19), the following coupling equation is obtained:

$$Mx'' + Kx = F - F_p \tag{22}$$

$$F_p = \int S\Big\{p_0(x)\Big\{n(x)[B]x_{(t)}\Big\}d_s\Big\} \tag{23}$$

where F_p is the acoustic force on the surface of the structure, S is the surface of the structure, $n(x)$ is the normal vector at a point on the surface, and $[B]$ is the matrix of the finite-element form functions.

The above equation describes the interaction between structural vibration and acoustic wave propagation. The coupling equation couples the kinetic vibration response data with the boundary element model to obtain the acoustic model, which can obtain the acoustic pressure data of the structural surface and acoustic wave propagation to study

the characteristics of the acoustic-structural coupling problem and complete the span from kinetics to acoustics.

6.2. Noise Measurement Methods

The sound pressure, decibels, and root mean square (RMS) values of the sound pressure level are all acoustic measures of the sound magnitude. Alternatively, the root mean square (RMS) values of sound pressure levels can provide more accurate and representative measurements. Because it averages all fluctuations of the sound and reflects the overall energy of the sound, it also provides more stable and reliable sound measurements by avoiding errors due to the instantaneous peaks in the sound. Therefore, the acoustic quantity used for noise detection is the root mean square (RMS) of the sound pressure level.

The relationship between the sound pressure, decibels, and root mean square (RMS) of the sound pressure level values can be expressed by the following equation:

$$dB = 10 \log 10^{(p/p_0)} \tag{24}$$

where dB is the decibel, p is the sound pressure of the sound to be measured, and p_0 is the reference sound pressure, usually taking a value of 20 micropascals (μPa), which is the reference level for human hearing.

The root mean square (RMS) value was calculated using the following equation:

$$RMS = \sqrt{\frac{1}{T}\int_o^T p(t)^2 \, dt} \tag{25}$$

where $p(t)$ is the sound pressure as a function of time and T is the period.

6.3. Actran-Based Vibroacoustic Analysis

ACTRAN software is a new generation of computational acoustics tools developed by FFT with a rich library of cells, materials, boundary conditions, problem-solving solutions, solvers, and pre- and post-processing interfaces. In this study, the analysis of vibro-acoustic radiation through the structure of a curved cylindrical gear pair is divided into three major steps: creation of the free-field model, creation of acoustic excitation, solution, and post-processing.

1. Creation of free-field model: import the finite element mesh model of the gear pair in ACTRAN, using the finite element mesh model, generate the acoustic boundary element mesh for the gear pair, and create the outer envelope according to Equation (16) to complete the creation of the free-field model, as shown in Figure 13.

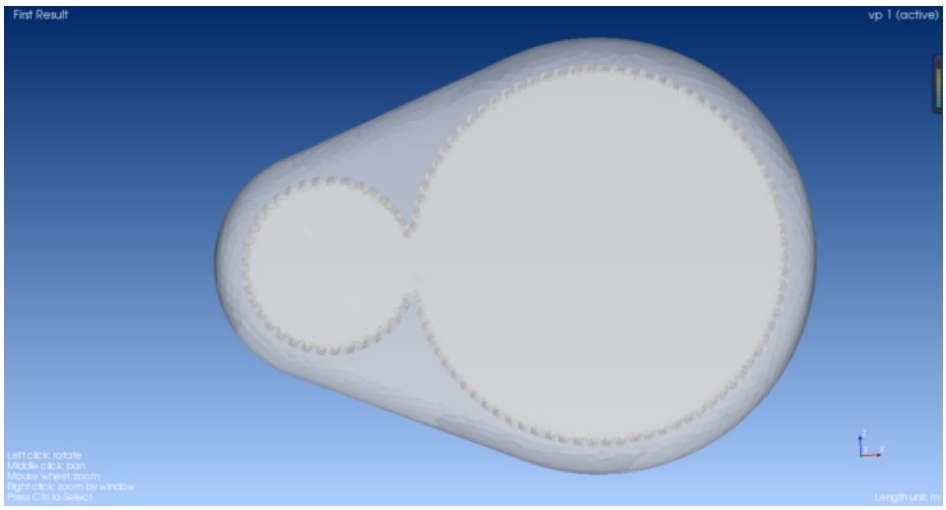

Figure 13. Free-field model.

2. According to Equations (20) and (23) for the creation of acoustic excitation, using direct frequency response analysis to solve, define the noise reflection boundary conditions for finite elements and boundary elements, and define the vibration coupling surface according to the results of the vibration response in ANSYS given to the acoustic vibration coupling surface. Considering that the passenger was located approximately 1 m directly above the traction gear train, the field point was set on the upper semicircular arc, approximately 1 m from the gear vice, to accurately predict the noise radiated from the passengers, as shown in Figure 14.

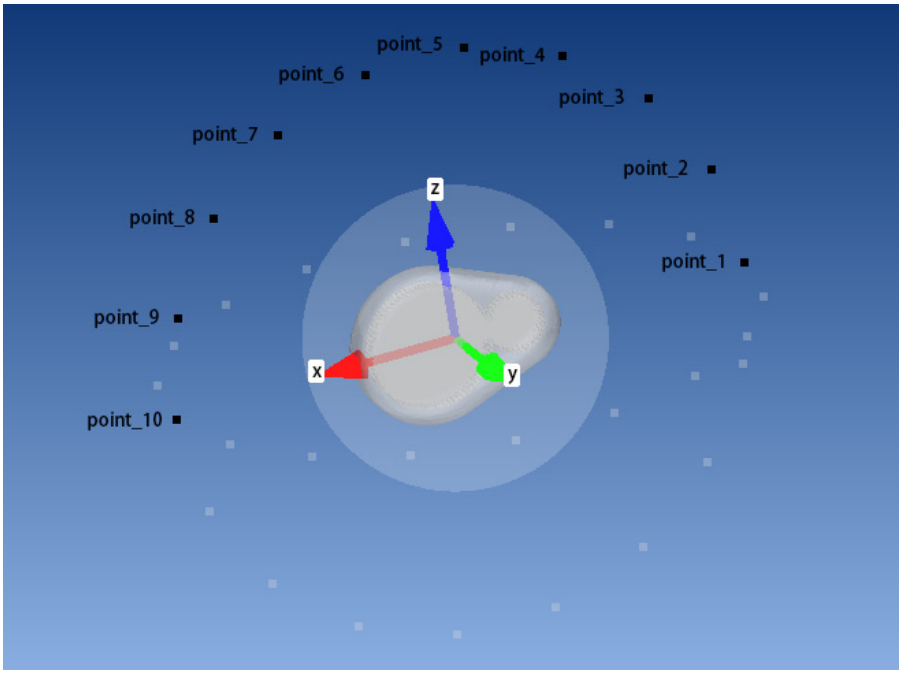

Figure 14. Acoustic field point distribution map.

3. According to Equation (20), Figure 15 shows the gear transmission radiation noise at each point on the sound pressure curve graph. According to Equation (21), the root-mean-square value of the radiated noise sound pressure level at each field point was calculated, as shown in Table 8.

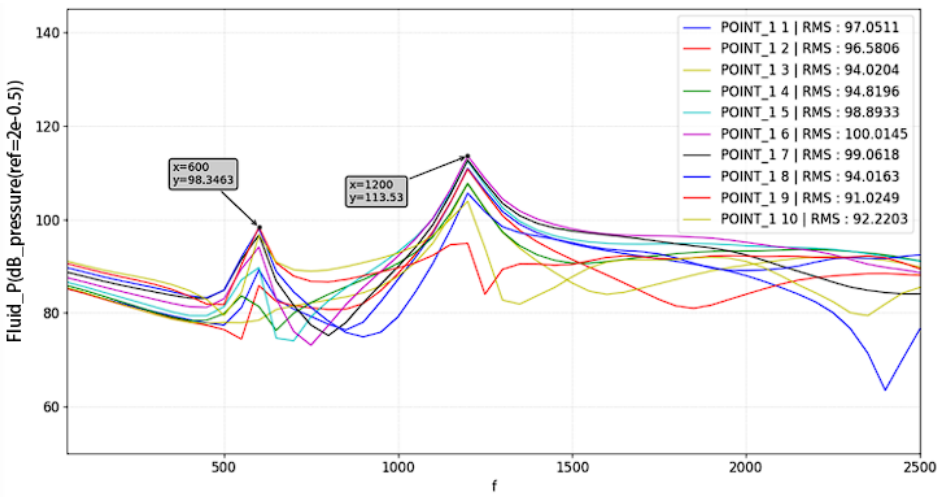

Figure 15. Sound pressure curve of each field point.

Table 8. RMS value of each field point (dB).

Field Point	RMS/dB	Field Point	RMS/dB
1	97.0511	6	100.0145
2	96.5806	7	99.0618
3	94.0204	8	94.0163
4	94.8196	9	91.0249
5	98.8933	10	92.2203

From the sound pressure, the curve can be seen from the arc tooth cylindrical gear transmission noise, which appears as a shoulder peak phenomenon, with the highest peak value of 113 Pa. Combined with the distribution of the field points, the RMS maximum point is located at field point POINT_6 above the gear, whose RMS is 100 dB, and the minimum point is located at the left field point POINT_9, whose RMS is 91 dB, which has lower noise than that reported in the literature [28]. The shoulder peak phenomenon is often caused by friction between the gear faces. To further verify this conjecture, the sound pressure clouds at these two frequencies were analyzed, as shown in Figures 16 and 17.

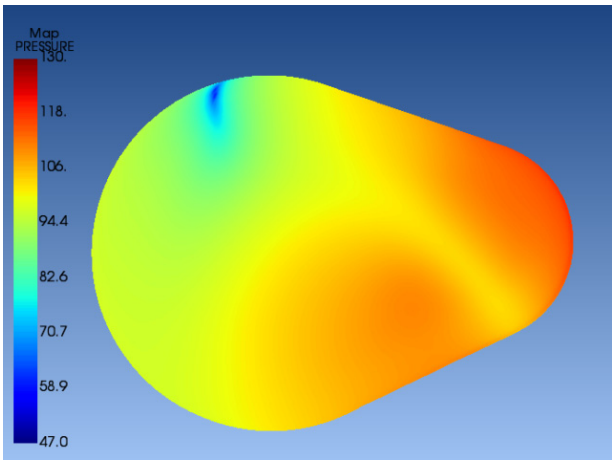

Figure 16. Sound pressure cloud at 600 Hz.

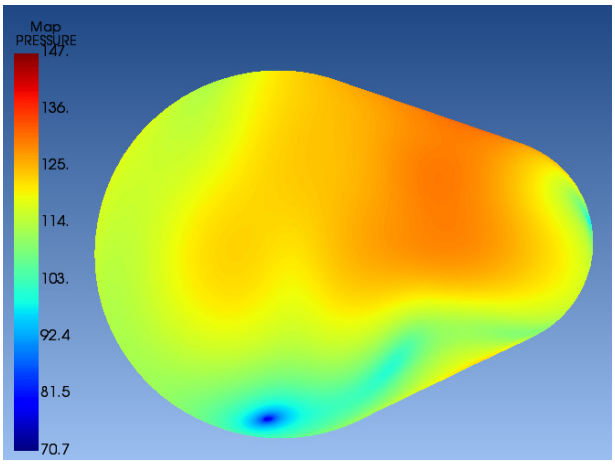

Figure 17. Sound pressure cloud at 1200 Hz.

An analysis of the sound pressure cloud indicated that the sound pressure at 600 Hz was concentrated at the upper-right side of the pinion and engagement below the gear pair with a maximum value of 130 Pa, and the sound pressure at 1200 Hz was concentrated at the engagement above the gear pair with a maximum value of 147 Pa. Areas with high peak values appear around the gear contact points, and it can be initially determined that

the shoulder peak phenomenon is caused by tooth surface friction. The intrinsic frequency of the gear pair successfully avoids the shoulder peak interval under continuous operating conditions, which can be further reduced by subsequent reshaping, indicating that the design of the curved cylindrical gear is reasonable and satisfies the noise requirements.

7. Conclusions

This study proposes a traction arc tooth cylindrical transmission gear pair that can be operated on a new-generation high-speed EMU. The parametric model of the curved cylindrical gear pair is constructed using CREO, and the results of the transient, modal, harmonic response, and vibro-acoustic analyses are as follows.

1. In the parametric modeling design of the curved cylindrical gear, the inner and outer edge curved lines are set on the indexing circle, and at the same time, the inner and outer edge curved lines are extended along the projection of the indexing circle, and then stretched in both directions to form a symmetrical drum-shaped distribution of tooth surface. This design makes the load distribution more uniform, effectively reduces the stress concentration on the top and bottom of the tooth, and increases the smoothness of the gear arc tooth orientation, thus improving the strength and transmission smoothness of the involute arc cylindrical gear and reducing the impact and noise.
2. The simulation analysis of the dynamics of the traction arc tooth cylindrical gear shows that the transmission error of the gear is 0.1516 μm in one meshing cycle, which indicates that the gear has a good meshing performance. The contact stresses were 595.9 MPa, 1677.9 MPa, and 172.14 MPa in engagement, meshing, and disengagement, respectively, and the distribution was relatively uniform and the contact line length was long, which reflected the high contact strength and load-bearing capacity of the gear. Owing to the curved design of the tooth surface, the shear stresses in the gear mesh appear in opposite directions on both sides of the tooth surface, so that they can cancel each other out. The comprehensive analysis results showed that the direction and magnitude of shear stresses changed at different stages during the meshing of the pinion and large gears and that the load distribution was more uniform, thus reducing the generation of meshing-in and meshing-out shocks and vibration noise. The displacement frequency response curve of the gear pair was obtained based on harmonic response analysis using the modal superposition method. These results are consistent with the situation in which the vibration in the gear transmission process presents a multiplicative frequency appearance. The analysis of the damping ratio and size of the critical damping ratio shows that the resonance phenomenon can be avoided.
3. Based on the dynamic response results, the vibration and radiated noise of the system under continuous operating conditions were solved using the direct frequency response analysis module of ACTRAN software. Several field points were set up at an upper arc of 1 m from the gear pair, and the noise radiation of the gear pair was analyzed in terms of both sound pressure and root mean square (RMS). The sound pressure curves at 600 Hz and 1200 Hz showed the shoulder peak phenomenon with the highest peak value of 113 Pa. Combining the sound pressure clouds of these two frequencies, it was found that the peak area was around the gear meshing, and the preliminary judgment was that the shoulder peak phenomenon was caused by tooth surface friction. The root mean square (RMS) was calculated for the sound pressure level value, and the distribution of the field points showed that the maximum RMS point was located at field point POINT_6 above the gear, with a value of 100 dB. The inherent frequencies of the large and small gears under continuous operation successfully avoided shoulder peak intervals. Through subsequent gear reshaping optimization, the traction gearbox noise will be controlled below the limit standard (100 dB (A)) specified in TB/T313402013 when operating under continuous

rated conditions, meeting the traction performance and vibration and noise reduction requirements of the new-generation high-speed EMU.

4. The paper focuses on proposing and designing arc tooth cylindrical gears to meet the demand of vibration and noise reduction in the traction system of a new generation of high-speed EMU, and adopts the finite element-boundary element method to simulate its dynamic characteristics and acoustic radiated noise, which theoretically verifies the feasibility of the model and method. The future research direction will also focus on the real operating environment of the traction gear drive system, and continue to explore the gear's multi-parameter combination of shape modification scheme, in order to further optimize the dynamic contact performance of the gear drive, and reduce the radiated noise of the gear drive. And with reference to the previous research results of the group and the cooperative unit about the locomotive current traction gear repair effect of the loading test ideas and methods [29], the simulation and analysis results of this paper need further experimental verification.

Author Contributions: Z.C.: methodology, formal analysis, writing—original draft, writing—review and editing, and data curation; Z.T.: validation, supervision, funding acquisition, and review; M.L.: data curation and editing; H.L.: data curation, formal analysis and editing; J.S.: data curation and editing. All authors have read and agreed to the published version of the manuscript.

Funding: This work was supported by the National Natural Science Foundation of China under Grant No. 52262049.

Informed Consent Statement: Informed consent was obtained from all subjects involved in the study.

Data Availability Statement: The data used in this study are available from the corresponding author upon request.

Conflicts of Interest: We declare that we do not have any commercial or associative interests that represent a conflict of interest in connection with the work submitted.

References

1. Wang, F. Building a new generation of CR450 high-speed trainsets with better performance to boost the development of China's high-speed rail industry in the 14th Five-Year Plan. *J. Urban Rail Transit Res.* **2022**, *25*, 10+144–145.
2. Chen, Z.; Zhai, W.; Wang, K. Locomotive dynamic performance under traction/braking conditions considering effect of gear transmissions. *J. Veh. Syst. Dyn.* **2018**, *56*, 1097–1117. [CrossRef]
3. Jiang, J.; Chen, Z.; Zhai, W. Vibration characteristics of railway locomotive induced by gear tooth root crack fault under transient conditions. *J. Eng. Fail. Anal.* **2020**, *108*, 104285. [CrossRef]
4. Wang, Z.; Yin, Z.; Wang, R. Coupled dynamic behaviour of a transmission system with gear eccentricities for a high-speed train. *J. Veh. Syst. Dyn.* **2021**, *59*, 613–634. [CrossRef]
5. Zhao, X.; Fan, W.; Wang, Z. An explicit finite element approach for simulations of transient meshing contact of gear pairs and the resulting wear. *J. Wear* **2023**, *523*, 204802. [CrossRef]
6. Yang, J.; Sun, R.; Yao, D. Nonlinear dynamic analysis of high speed multiple units gear transmission system with wear fault. *J. Mech. Sci.* **2019**, *10*, 187–197. [CrossRef]
7. Yavuz, S.D.; Saribay, Z.B.; Cigeroglu, E. Nonlinear dynamic analysis of a drivetrain composed of spur, helical and spiral bevel gears. *J. Nonlinear Dyn.* **2020**, *100*, 3145–3170. [CrossRef]
8. Sun, G.; Ren, Z.S.; Xin, X. Vibration characteristics of high-speed rolling stock gearing systems. *J. Mech. Eng.* **2020**, *55*, 104–111.
9. Tang, Z.; Wang, M.; Hu, Y. Optimal design of traction gear modification of high-speed EMU based on radial basis function neural network. *J. IEEE Access* **2020**, *8*, 134619–134629. [CrossRef]
10. Zhang, T.; Chen, Z.; Zhang, J. Effect of motor suspension parameters on dynamic characteristics of gear transmission system in a locomotive. In Proceedings of the First International Conference on Rail Transportation 2017, Reston, VA, USA, 10–12 July 2017; pp. 576–585.
11. Zhu, W.; Lin, H.; Sun, W.; Wei, J. Vibration Performance of Traction Gearbox of a High-Speed Train: Theoretical Analysis and Experiments. *Actuators* **2023**, *12*, 103. [CrossRef]
12. Liu, L.; Kang, K.; Xi, Y. Optimal Design and Experimental Verification of Low Radiation Noise of Gearbox. *J. Chin. J. Mech. Eng.* **2022**, *35*, 130. [CrossRef]
13. Ren, Y.; Chang, S.; Liu, G. Numerical Noise Transfer Analysis of a Flexible Supported Gearbox Based on Impedance Model and Noise Transfer Function. *J. Math. Probl. Eng.* **2020**, *2020*, 1294609. [CrossRef]

14. Tengjiao, L.; Zeyin, H.; Feiyu, G. Prediction and experimental study on structure and radiation noise of subway gearbox. *J. Vibroeng.* **2013**, *15*, 1838–1846.
15. Han, J.; Liu, Y.; Yu, S. Acoustic-vibration analysis of the gear-bearing-housing coupled system. *J. Appl. Acoust.* **2021**, *178*, 108024. [CrossRef]
16. Gunasegaran, V.; Amarnath, M.; Chelladurai, H. Assessment of local faults in helical geared system using vibro-acoustic signals based on higher order spectrum analysis. *J. Appl. Acoust.* **2023**, *204*, 109237. [CrossRef]
17. Feng, K.; Ji, J.C.; Zhang, Y.; Ni, Q.; Liu, Z.; Beer, M. Digital twin-driven intelligent assessment of gear surface degradation. *Mech. Syst. Signal Process.* **2023**, *186*, 109896. [CrossRef]
18. Feng, K.; Xu, Y.; Wang, Y.; Li, S.; Jiang, Q.; Sun, B.; Ni, Q. Digital Twin Enabled Domain Adversarial Graph Networks for Bearing Fault Diagnosis. *IEEE Trans. Ind. Cyber-Phys. Syst.* **2023**, *1*, 113–122. [CrossRef]
19. Mu, Y.; He, X. Design and dynamic performance analysis of high-contact-ratio spiral bevel gear based on the higher-order tooth surface modification. *J. Mech. Mach. Theory* **2021**, *161*, 104312. [CrossRef]
20. Yuan, B.; Liu, G.; Yue, Y. A novel tooth surface modification methodology for wide-faced double-helical gear pairs. *J. Mech. Mach. Theory* **2021**, *160*, 104299. [CrossRef]
21. Li, H.; Tang, J.; Chen, S. Loaded contact pressure distribution prediction for spiral bevel gear. *J. Int. J. Mech. Sci.* **2023**, *242*, 108027. [CrossRef]
22. Chen, W.; Chen, S.; Hu, Z. A novel dynamic model for the spiral bevel gear drive with elastic ring squeeze film dampers. *J. Nonlinear Dyn.* **2019**, *98*, 1081–1105. [CrossRef]
23. Li, Z.; Wang, S.; Li, L. Study on multi-clearance nonlinear dynamic characteristics of herringbone gear transmission system under optimal 3d modification. *J. Nonlinear Dyn.* **2023**, *111*, 4237–4266. [CrossRef]
24. Zou, H.; Wang, S.; Li, F. Improved algorithm of tooth surface topological modification and nonlinear dynamic analysis of herringbone gears. *J. Mech. Mach. Theory* **2023**, *180*, 105151. [CrossRef]
25. Zhijun, S.; Li, H.; Jinge, W. Contact strength analysis of circular-arc-tooth-trace cylindrical gear. *J. Braz. Soc. Mech. Sci. Eng.* **2016**, *38*, 999–1005. [CrossRef]
26. Syzrantseva, K.; Syzrantsev, V.; Babichev, D. *Comparative Analysis of Stress–Strain Condition of Cylindrical Gears Arc Teeth and Spurs: ICIE 2019*; Springer International Publishing: Berlin/Heidelberg, Germany, 2020; pp. 101–108.
27. Syzrantseva, K.V.; Syzrantsev, V.N.; Kolbasin, D.S. Comparative estimation of the failure probability of cylindrical arc and helical gears by tooth bending endurance. In Proceedings of the AIP Conference Proceedings, Ekaterinburg, Russia, 19 November 2019; Volume 2176, p. 020010.
28. Tang, Z.P.; Chen, Z.X.; Sun, J.P. Noise prediction of traction gear in high-speed electric multiple unit. *J. Int. J. Simul. Model.* **2019**, *18*, 720–731. [CrossRef]
29. Yan, L.; Zhang, P.F.; Tang, Z.P. Analysis of the effect of different spoke plate structures on the tooth contact of locomotive traction gears. *J. Shijiazhuang Railw. Univ. (Nat. Sci. Ed.)* **2019**, *32*, 66–70.